Placing limits on the stochastic gravitational-wave background using European Pulsar Timing Array data

R. van Haasteren,[1]⋆ Y. Levin,[2,1] G. H. Janssen,[3] K. Lazaridis,[4] M. Kramer,[4,3]
B. W. Stappers,[3,5] G. Desvignes,[6,7,8] M. B. Purver,[3] A. G. Lyne,[9]
R. D. Ferdman,[6,7] A. Jessner,[4] I. Cognard,[6,7] G. Theureau,[6,7] N. D'Amico,[10,11]
A. Possenti,[11] M. Burgay,[11] A. Corongiu,[11] J. W. T. Hessels,[5,12] R. Smits[3,5]
and J. P. W. Verbiest[4]

[1]*Leiden Observatory, Leiden University, PO Box 9513, NL-2300 RA Leiden, the Netherlands*
[2]*School of Physics, Monash University, PO Box 27, VIC 3800, Australia*
[3]*University of Manchester, Jodrell Bank Centre for Astrophysics, Alan Turing Building, Manchester M13 9PL*
[4]*Max-Planck-Institut für Radioastronomie, Auf dem Hügel 69, 53121 Bonn, Germany*
[5]*Netherlands Institute for Radio Astronomy (ASTRON), Postbus 2, 7990 AA Dwingeloo, the Netherlands*
[6]*LPC2E, Université d'Orléans - CNRS, 3A Av de la Recherche Scientifique, F45071 Orléans Cedex 2, France*
[7]*Station de Radioastronomie de Nançay, Observatoire de Paris, CNRS/INSU, F18330 Nançay, France*
[8]*Department of Astronomy and Radio Astronomy Laboratory, University of California, Berkeley, CA 94720, USA*
[9]*University of Manchester, Jodrell Bank Observatory, Macclesfield, Cheshire, SK11 9DL*
[10]*Dipartimento di Fisica, Università Degli Studi di Cagliari, SP Monserrato-Sestu km 0.7, 90042 Monserrato (CA), Italy*
[11]*INAF Osservatorio Astronomico di Cagliari, Loc. Poggio dei Pini, Strada 54, 09012 Capoterra (CA), Italy*
[12]*Astronomical Institute 'Anton Pannekoek', University of Amsterdam, 1098 SJ Amsterdam, the Netherlands*

ABSTRACT

Direct detection of low-frequency gravitational waves (GWs, 10^{-9} to 10^{-8} Hz) is the main goal of pulsar timing array (PTA) projects. One of the main targets for the PTAs is to measure the stochastic background of gravitational waves (GWB) whose characteristic strain is expected to approximately follow a power-law of the form $h_c(f) = A(f/\text{yr}^{-1})^\alpha$, where f is the GW frequency. In this paper we use the current data from the European PTA to determine an upper limit on the GWB amplitude A as a function of the unknown spectral slope α with a Bayesian algorithm, by modelling the GWB as a random Gaussian process. For the case $\alpha = -2/3$, which is expected if the GWB is produced by supermassive black hole binaries, we obtain a 95 per cent confidence upper limit on A of 6×10^{-15}, which is 1.8 times lower than the 95 per cent confidence GWB limit obtained by the Parkes PTA in 2006. Our approach to the data analysis incorporates the multitelescope nature of the European PTA and thus can serve as a useful template for future intercontinental PTA collaborations.

Key words: gravitational waves – methods: data analysis – pulsars: general.

1 INTRODUCTION

The first direct detection of gravitational waves (GWs) would be of great importance to astrophysics and fundamental physics: it would confirm some key predictions of general relativity, and lay the foundation for observational GW astronomy. Pulsar timing arrays (PTAs) are collaborations which aim to detect low-frequency (10^{-9} to 10^{-8} Hz) extragalactic GWs directly, by using a set of Galac-

⋆E-mail: haasteren@strw.leidenuniv.nl
There is an Erratum to this article at doi:10.1111/j.1365-2966.2012.20916.x.

tic millisecond pulsars as nearly perfect Einstein clocks (Foster & Backer 1990). The basic idea is to exploit the fact that millisecond pulsars create pulse trains of exceptional regularity. GWs perturb Space–time between the pulsars and the Earth, and this creates detectable deviations from the strict periodicity in the arrival times of the pulses (TOAs) (Estabrook & Wahlquist 1975; Sazhin 1978; Detweiler 1979).

One of the main astrophysical targets of the PTAs is to measure the stochastic background of gravitational waves (GWB). This GWB is expected to be generated by a large number of black hole binaries located at the centres of galaxies (Begelman, Blandford &
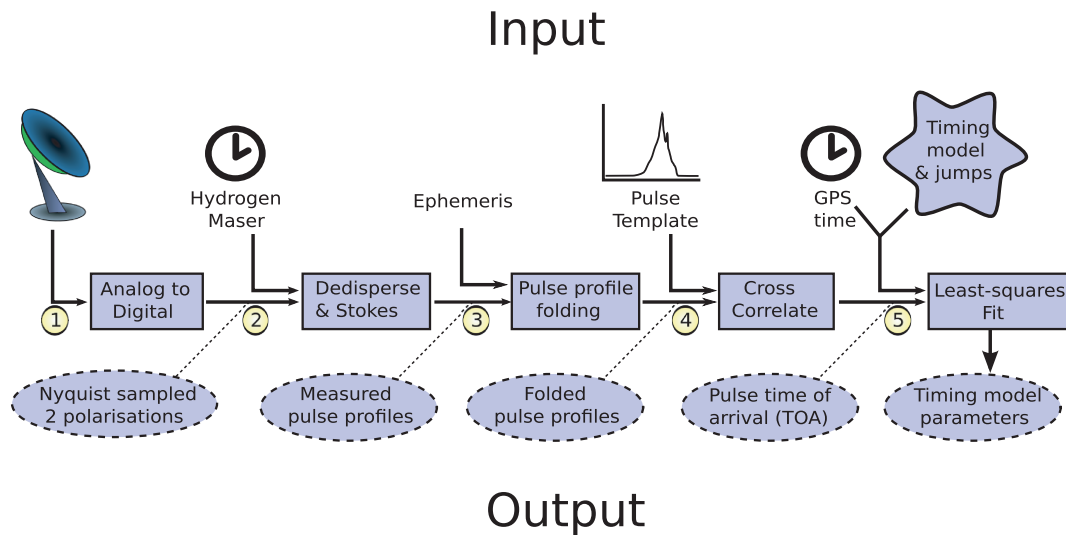
Input

Output

Figure 1. The processing pipeline for pulsar timing, step by step.

Rees 1980; Phinney 2001; Jaffe & Backer 2003; Wyithe & Loeb 2003; Sesana, Vecchio & Colacino 2008), by relic BWs (Grishchuk 2005), or, more speculatively, by oscillating cosmic-string loops (Damour & Vilenkin 2005; Ölmez, Mandic & Siemens 2010).

Currently, there are three independent PTA groups.

(i) The Australian-based programme PPTA, the Parkes PTA, which uses data from the Parkes Telescope (Hobbs et al. 2009; Verbiest et al. 2010) and archival Arecibo data.

(ii) The North-American based programme NANOGrav, North-American Nanohertz Observatory for GWs, which uses both the Green Bank Telescope (GBT) and the Arecibo radio telescope (Jenet 2009).

(iii) And the European programme European PTA (EPTA) which uses five different radio telescopes: the Lovell telescope near Manchester, United Kingdom, the Westerbork Synthesis Radio Telescope (WSRT) in the north of the Netherlands, the Effelsberg Telescope (EFF) near Bonn in Germany, the Nançay Radio Telescope (NRT) near Nançay in France and the Sardinia Radio Telescope (SRT) in Sardinia, Italy.[1]

It is likely that the first detection of GWs by a PTA will occur as a result of a joint effort of all current PTA projects: an International Pulsar Timing Array (IPTA; Hobbs et al. 2010). This will involve the combination of data from several different telescopes, each of them with its own specific hardware elements and software analysis tools. Combining data of different observatories is a challenging task, which requires extra care when dealing with the high-quality data of modern observatories (Janssen 2009).

In this EPTA paper, we present a methodology on how to combine the data from several radio telescopes and use it in an optimal way to obtain the information on extragalactic GWs. We use the data from three different radio telescopes located on the European continent, to place a new upper limit on the amplitude of the GWB. As part of our analysis, we obtain detailed information about the statistical properties of the individual pulse time series.

The calculation of upper limits on the GWB, based on pulsar timing, go as far back as the early 1990's (Stinebring et al. 1990; Kaspi, Taylor & Ryba 1994; McHugh et al. 1996; Lommen 2002).

These analyses have been based on high quality data sets for single millisecond pulsars. The most stringent upper limits have been obtained recently by Jenet et al. (2006), who have used PPTA data and archival Arecibo data for several millisecond pulsars. Our data set is different from that used by Jenet et al. (2006) since it includes only the pulse times of arrival measured by the EPTA Telescopes, even though some of the pulsars are being timed by multiple PTA groups. The Bayesian algorithm we use to obtain an upper limit on the GWB is also different from the algorithms used by all of the previous studies. Its potential advantages include the use of cross correlations between TOAs of different pulsars, and the simultaneous constraint on both the amplitude and spectral index of the GWB.

The outline of the paper is as follows. In Section 2 we give a brief general overview of pulsar timing observations. In Section 3 we detail the observations from all of the EPTA telescopes which were used for this paper's analysis. We outline the data analysis procedure in Section 4, after which, in Section 5, we present the upper limits on the amplitude of the GWB, and also the spectral analysis of the individual pulsar noises. Finally, in Section 6 we discuss the astrophysical implications of our results.

2 EPTA DATA ANALYSIS

In this section we present a brief overview of the observations, instrumentation and data analysis used at the different EPTA observatories for transforming a series of measured pulses to a TOA.

The complete data reduction process that converts the incoming data stream from a radio telescope into one single TOA per observation, called 'the pipeline', is optimized by hand with much care and is observatory specific. The process can be described in five general steps, shown in Fig. 1:

(1) the incoming radio waves are received by the telescope,

(2) the signal is converted from analog to digital, at a Nyquist sampled rate,

(3) data are (coherently) dedispersed and, if possible, Stokes parameters are formed,

(4) the dedispersed time-series are folded at the pulsar period, resulting in averaged pulse profiles. Typically a time span containing several 10^5 pulses is used for each TOA,

---

[1] The SRT is expected to become operational in 2011 (Tofani et al. 2008).

(5) a cross-correlation with a template pulse profile yields a TOA and associated uncertainty (Taylor 1992).

Individual pulse amplitudes and pulse shapes are highly irregular, and pulse phases vary significantly from pulse to pulse (Cordes & Shannon 2010). Therefore careful averaging *(folding)* has to be performed to obtain a single TOA. Furthermore, the interstellar medium (ISM) results in significant delays of the arrival time of the pulses over the receiver bandwidth. As a large bandwidth is required to reliably detect a pulse, accounting for the ISM is key for precision timing.

Differences in templates used, e.g. the use of integrated profiles versus analytic templates, all based on single-observatory data, and the difference in definition of the reference point in a template will result in offsets between data sets generated by different observatories. All extra offsets in our data will lead to information loss of other signals like the GWB. Therefore, using a common template for each pulsar at all observatories is desirable, and will be implemented in the near future.

The realization of the five steps and therefore their output (the resulting TOA) might differ among observatories. Understanding and accounting for those differences is essential for the correct analysis and optimal combining of the EPTA data. A more detailed study on this subject is in preparation (Janssen et al., in preparation).

The cross-correlation between the folded profile and the template yields an uncertainty of the TOA (Taylor 1992). One would like this uncertainty to be solely due to the radiometre noise, i.e. the noise intrinsic to the measurement, but in practice the errors sometimes appear to have been systematically over- or under-estimated. It is a common practice, which we follow here, to allow for an extra parameter to multiply these uncertainties for each pulsar-observatory-backend combination (Hobbs & Edwards 2006). This extra multiplicative factor allows the TOA uncertainties to statistically account for the TOA scatter: the deviations of the strict periodicity of the pulses. This is clearly unsatisfactory, and in future timing experiments the origin of the predicted and measured TOA scatter will have to be thoroughly investigated.

3 EPTA OBSERVATIONS

3.1 Overview of the observatories

We have used pulsar timing observations of five radio pulsars, observed with three of the EPTA telescopes, to set a limit on the GWB. See Table 1, Fig. 2 and the appendix for an overview of the data sets used and the properties of each telescope. Each pulsar was observed on average once every month for 30 min at each telescope. Although additional observing frequencies are commonly used at WSRT and EFF, their respective 1380- and 1400-MHz observing bands have the best sensitivity and result in the highest precision
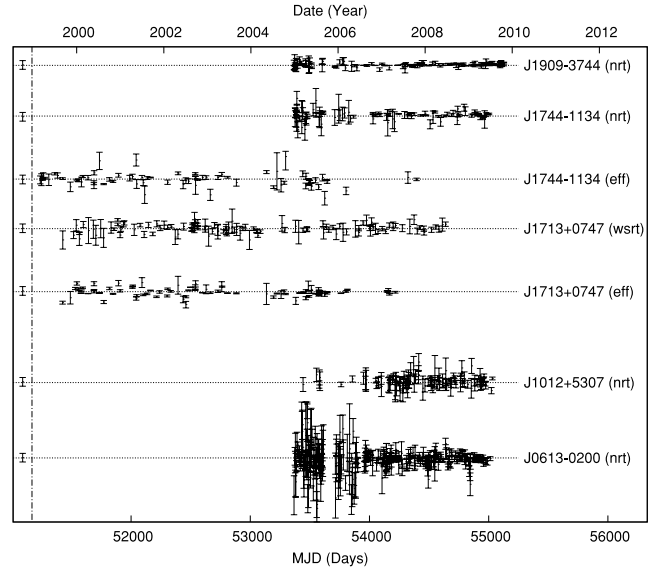

Figure 2. The timing residuals of all the pulsars used in the GWB limit calculation. The time in MJD is shown on the *x*-axis. On the left of the dot–dashed line we have placed a sample residual with an uncertainty of 1 μs.

TOAs. Therefore we have only used observations taken at those frequencies at WSRT and EFF for the analysis presented in this paper. The data were either coherently dedispersed (NRT and EFF) or incoherently dedispersed (WSRT). The observations were folded and cross-correlated with an analytic template (EFF), or a high signal to noise ratio, observatory specific, template (WSRT and NRT), to calculate one time-of-arrival (TOA) per observation. See e.g. Lazaridis et al. (2009) for a more complete description of the observing procedures and data analysis at the different observatories.

As discussed, any change to the pipeline or to the input of the pipeline can result in a difference in the calculated TOAs. We emphasize that it is essential to correctly identify these systematic effects and include them in the modelling of the TOAs. In our analysis, we have done this by introducing jumps between TOAs of the same pulsar anywhere the pipeline differs in some way.

Once the complete set of data for each pulsar is obtained, and corrected for global drifts by comparing to UTC, it is fit with the timing model. The timing model is a multiparameter fit that represents our best knowledge of the many deterministic processes that influence the values of the TOAs. The timing residuals are then produced by subtracting the timing model, which is subsequently optimized by minimizing these residuals through a least-squares fit. This was done using the pulsar timing package TEMPO2 (Hobbs, Edwards & Manchester 2006).

Table 1. Details of the different EPTA observatories relevant for this work. The NRT observing bandwidth has doubled to 128 MHz in 2009 July.

Telescope	WSRT	NRT	EFF
Equivalent dish size (m)	93.5	94.4	100
Centre observing frequencies (MHz)	1380	1398, 2048	1400
Observing bandwidth (MHz)	80	64/128	28–112
Obs. time per month per pulsar	1×30 min	4–6×60 min	1×30 min
Pulsar backend	PuMaI	BON	EBPP
Dedispersion	incoherent	coherent	coherent
Used templates	integrated profiles	integrated profiles	analytic

3.2 Selection of data sets

The European observatories have been timing millisecond pulsars for many years, and potentially all of that data could be used in the calculation of an upper limit on the GWB. However, like Jenet et al. (2006) we choose to use only the data from the pulsars which perform best as ideal clocks, e.g. those with the highest precision TOAs and the most straight-forward noise characteristics.

TOA precision is not the only factor that determines the sensitivity to the GWB; other factors like the total timing baseline and the number of observations (i.e. TOAs) affect this sensitivity as well. A great advantage of the EPTA data is that several pulsars have been monitored for a relatively long time: over 10 yr. To determine which timing residuals (i.e. pulsar-observatory combinations) are most useful for GWB detection, we analyse each data set separately. By doing this we can determine the sensitivity to the GWB of a set of TOAs: the lower the 3σ upper limit $h_c^{\max}(1\,\mathrm{yr})$ we get using only a particular set of TOAs, the more sensitive that set of TOAs is to the GWB.

The timing residuals of the selected pulsars are shown in Fig. 2. These five pulsars significantly outperform the other pulsars being timed by the EPTA in terms of how well they can limit the GWB amplitude: these five pulsars can each individually limit the GWB well below $h_c(1\,\mathrm{yr}) = 10^{-13}$ for $\alpha = -2/3$, whereas other current EPTA data sets typically perform worse by a factor of several. Since there is such a difference between this set of five pulsars, and the other pulsars that have been observed by the EPTA, we do not expect to gain any significant sensitivity by including more pulsars that cannot meet this constraint. We therefore choose $h_c^{\max}(1\,\mathrm{yr}) \leq 10^{-13}$ with $\alpha = -2/3$ as a constraint for including a data set in our calculation.

In addition to this constraint, we also demand that data sets that just barely satisfy $h_c^{\max}(1\,\mathrm{yr}) \leq 10^{-13}$ do not show prominent low-frequency ('red') timing noise. Our criterion for presence of the latter is a peak in the posterior distribution which is inconsistent with zero amplitude for $\alpha \leq 0$.

4 DATA ANALYSIS

The analysis presented in this paper broadly follows the procedure introduced in van Haasteren et al. (2009, vHLML). The vHLML Bayesian algorithm relies on creating the parametrized models of the timing residuals, and forming a probability distribution function (PDF) as a function of the model parameters. All known systematic contributions of known functional form should be included in the model. In the examples used by vHLML the model for the systematic errors included only the quadratic contribution to the TOAs from pulsar spin-downs. The multitelescope nature of the EPTA requires more complete models for timing residuals than the one used in vHLML. In this section we show how to build and implement these models in practice.

We first briefly review the algorithm of vHLML in Section 4.1 and 4.2. We then present the extended model we use for the analysis of the TOAs in Section 4.3, after which we show how we handle TOAs coming from different observatories in Section 4.4.

4.1 Brief review of the vHLML algorithm

The set of TOAs from all pulsars forms the basic input used in the Bayesian data analysis. Many processes influence the measured TOA values; in this work we discriminate between deterministic processes, like quadratic spin-down, and stochastic processes, like timing noise:

$$t_{(ai)}^{\mathrm{obs}} = t_{(ai)}^{\mathrm{det}} + \delta t_{(ai)}^{\mathrm{stoch}}, \qquad (1)$$

where $t_{(ai)}^{\mathrm{obs}}$ represents the ith TOA of pulsar a, $t_{(ai)}^{\mathrm{det}}$ is the corresponding contribution to the TOA solely due to deterministic processes, and $\delta t_{(ai)}^{\mathrm{stoch}}$ is the contribution due to stochastic processes.

The effects of deterministic processes are described by the set of model parameters η: $t_{(ai)}^{\mathrm{det}} = t_{(ai)}^{\mathrm{det}}(\eta)$. As is done in vHLML, we assume that the stochastic processes are Gaussian, though their spectra are not necessarily white. In such a model, the stochastic processes can be represented by the correlation matrix

$$\left\langle \delta t_{(ai)}^{\mathrm{stoch}} \delta t_{(bj)}^{\mathrm{stoch}} \right\rangle = C_{(ai)(bj)} = C_{(ai)(bj)}(\boldsymbol{\xi}), \qquad (2)$$

where $\boldsymbol{\xi}$ are the model parameters.

The key distribution used in a Bayesian analysis is the likelihood function, the probability distribution of the data for a given model and its parameters. As described in vHLML, for PTAs the likelihood takes the following form:

$$L(\boldsymbol{\theta}) = P(\boldsymbol{\delta t} \,|\, \boldsymbol{\theta}) = \frac{1}{\sqrt{(2\pi)^n \det C}}$$
$$\times \exp\left[-\frac{1}{2} \sum_{(ai)(bj)} \left(t_{(ai)}^{\mathrm{obs}} - t_{(ai)}^{\mathrm{fit}} \right) C_{(ai)(bj)}^{-1} \left(t_{(bj)}^{\mathrm{obs}} - t_{(bj)}^{\mathrm{fit}} \right) \right], \qquad (3)$$

where $\boldsymbol{\theta} = (\boldsymbol{\eta}, \boldsymbol{\xi})$, and $\boldsymbol{\delta t}$ is the difference between the observed TOAs, and the fitted TOAs. A Bayesian analysis assigns prior distributions $P_0(\boldsymbol{\theta})$ to the model parameters, and explores the parameter space of the posterior distribution (short-handed simply as the posterior): $P(\boldsymbol{\theta} \,|\, \boldsymbol{\delta t}) = L(\boldsymbol{\theta}) P_0(\boldsymbol{\theta})$.

4.2 Obtaining a marginalized posterior distribution

The posterior $P(\boldsymbol{\theta} \,|\, \boldsymbol{\delta t})$ contains information about all model parameters. We need to express the posterior as a function of only those parameters that represent the GWB. This process is called marginalization, and consists of integrating over all other parameters. The resulting marginalized posterior is the posterior probability density of the GWB parameters.

Marginalization of a posterior in a high-dimensional parameter space is non-trivial, and a direct numerical integration is prohibitively computationally expensive. As in vHLML, we employ a mix of analytic integration and Markov Chain Monte Carlo (MCMC) methods to accomplish this. The marginalization remains the computational bottleneck for the method's effectiveness, as the computational time scales with n^3, with n the total number of TOAs to be analysed.

A computational shortcut can be used by analytically marginalizing over the parameters of the timing model. As shown in vHLML, this is possible provided that the parameters represent signals of known functional form. This condition is equivalent to the requirement that the timing residuals generated by the timing model are linear with respect to its parameters: $\delta t = \mathrm{d}(\alpha - \hat{\alpha})$, where δt is the timing residual, d is a proportionality constant, $\hat{\alpha}$ is the best-fitting value for the model parameter and α is the model parameter. While this is always true for quadratic spin-down as considered explicitly in vHLML, it is generally not true for other timing model parameters. However, when the deviations of the timing model parameters from their best-fitting values are small, it is a good approximation that the residuals generated by the timing model are linear with respect to the deviations from their best-fitting values: $\delta t \approx \mathrm{d}(\alpha - \hat{\alpha})$.

Analytically marginalizing over the timing model is therefore possible, and by doing so the number of parameters that must be

integrated over numerically by the use of MCMC is reduced greatly. Dependent on the model we use to describe the statistics of the timing residuals, the number of parameters left to explore is then just several per pulsar/backend combination. The results of the analysis can be presented as a marginalized posterior as a function of any parameter in the model, provided that this parameter was present in the MCMC run.

4.3 Used model for the TOAs

We divide the actual parametrization in three parts:

   (a) The deterministic timing model.
   (b) The GW background.
   (c) Other stochastic processes (e.g., timing noise).

In this section we discuss how we have taken these into account in our data analysis.

As a first step, the TOAs are processed using the software package TEMPO2, in order to determine the best-fitting timing model. This procedure consists of the following steps:

   (1) TEMPO2 requires an initial guess α_{0i} for the timing model parameters α_i in order to find timing residuals (pre-fit timing residuals).

   (2) It then constructs an approximation to the timing model, in which the timing residuals depend linearly on $\alpha_i - \alpha_{0i}$.

   (3) It finds the best-fitting α_i within this linear approximation, and uses those values to update the timing residuals using the full non-linear timing model (post-fit timing residuals).

   (4) The newly obtained parameters and corresponding timing residuals are then judged by the person performing the model fitting, and if determined necessary the newly obtained parameters can act as the initial guess for a new fitting iteration. TEMPO2 also allows adjustment and fitting of α_i one by one.

Finding the timing solution with TEMPO2 is not fully algorithmic, but typically requires someone experienced with pulsar timing analysis, who approaches the TOAs fitting in several different ways, which ensures that phase coherence is maintained and that the relevant deterministic model parameters are included properly. Though this strategy works well in practice, we should remain conscious of the possibility that different solutions might be obtained by different observers, who may also choose to include additional model parameters.[2] In the appendix we present the timing solutions we found for the analysed pulsars. These are the values we used as our initial guess, α_{0i}. Note that these α_{0i} and their uncertainties, although created with TEMPO2 using the same data sets that we base our upper limit on, do not include our model for the red noise. The values and uncertainties we list in the appendix therefore do not represent our best estimates if we were to take into account the red timing noise. Although calculating these best estimates of α_i is reasonably straightforward, these estimates are not accessible in our MCMC because we have marginalized over these parameters analytically. The calculated upper limit on the GWB, however, does include all these effects, and therefore automatically incorporates

the removal of power from the low-frequency GW signal by fitting for the timing model parameters and jumps.

In the above mentioned step 2 where the timing model is linearized, we have made an important simplification that we now describe in more detail. Since we take into account, and marginalize over, all timing model parameters in our algorithm, we are effectively working with the TOAs instead of just the timing residuals. However, the timing model has been linearized by TEMPO2 with respect to $\alpha_i - \alpha_{0i}$. This implies that we need to be sufficiently close to α_{0i} in the parameter space for this approximation to be valid, which means that the timing residuals derived with TEMPO2 need to be approved by the person fitting the data, before using these as inputs in the Bayesian algorithm.

The stochastic component contributing to the TOAs is characterized as follows. First, general relativity describes how the timing residuals of a pair of pulsars are correlated due to GWs:

$$\zeta_{ab} = \frac{3}{2} \frac{1 - \cos\theta_{ab}}{2} \ln\left(\frac{1 - \cos\theta_{ab}}{2}\right) - \frac{1}{4}\frac{1 - \cos\theta_{ab}}{2} + \frac{1}{2} + \frac{1}{2}\delta_{ab},$$ (4)

where θ_{ab} is the angle between pulsar a and pulsar b (Hellings & Downs 1983). The GWB spectrum is parametrized as a power law of the form (Maggiore 2000; Phinney 2001; Jaffe & Backer 2003; Wyithe & Loeb 2003; Sesana et al. 2008):

$$h_c = A\left(\frac{f}{\mathrm{yr}^{-1}}\right)^\alpha,$$ (5)

were h_c is the characteristic strain as used in Jenet et al. (2006), A is the amplitude of the signal, and α is the spectral index. This then results in a correlation matrix for the GWB (vHLML):

$$C_{(ai)(bj)}^{\mathrm{GW}} = \frac{-A^2\zeta_{ab}}{(2\pi)^2 f_L^{2-2\alpha}}\left\{\Gamma(-2 + 2\alpha)\cos(\pi\alpha)(f_L\tau)^{2-2\alpha}\right.$$
$$\left. \times \sum_{n=0}^\infty (-1)^n \frac{(f_L\tau)^{2n}}{(2n)!\,(2n + 2\alpha - 2)}\right\},$$ (6)

where, as in vHLML, $\tau = 2\pi|t_i - t_j|$, and f_L is a cut-off frequency, set much lower than the lowest GW frequency we are sensitive to.

Secondly, the stochastic timing noise for each individual pulsar is split into three components:

   (1) Individual errors of TOA determination from the cross-correlation, represented by the TOA error bars. An extra free parameter, called the EFAC value, is commonly introduced by pulsar observers in order to account for possible miscalibration of the radiometre noise (Hobbs & Edwards 2006); this parameter is a multiplier for all of the TOA error bars for a given pulsar.

   (2) An extra white noise component, independent of the error bars. This basically acts as extra non-time-dependent noise, and the parameter is often called an EQUAD parameter.

   (3) Red noise, consisting of a power-law spectrum in the timing residuals. This component allows for structure in the timing residuals.

All three timing noise components are uncorrelated between the pulsars.

---

[2] Qualitatively, experienced observers are rightfully so very confident in their timing solutions. Quantitatively, however, the only statistical tool currently available for observers to check whether the timing solution is reasonable is the reduced χ^2 statistic. But since the error bars obtained with the cross-correlation technique cannot be fully trusted, the same holds for the χ^2 statistic.

The resulting correlation matrices from components 1, 2 and 3, as derived in vHLML, are given by:

$$C_{(ai)(bj)}^{\mathrm{err}} = E_a^2 \Delta t_{(ai)}^2 \delta_{ab} \delta_{ij}$$

$$C_{(ai)(bj)}^{\mathrm{WN}} = N_a^2 \delta_{ab} \delta_{ij}$$

$$C_{(ai)(bj)}^{\mathrm{RN}} = \frac{-R_a^2 \delta_{ab}}{(2\pi)^2 f_L^{2-2\alpha_a}} \left\{ \Gamma(-2 + 2\alpha_a) \cos(\pi\alpha_a) (f_L \tau)^{2-2\alpha_a} \right.$$

$$\left. \times \sum_{n=0}^{\infty} (-1)^n \frac{(f_L \tau)^{2n}}{(2n)! (2n + 2\alpha - 2)} \right\}, \tag{7}$$

where $C_{(ai)(bj)}^{\mathrm{err}}$, $C_{(ai)(bj)}^{\mathrm{WN}}$ and $C_{(ai)(bj)}^{\mathrm{RN}}$ are the correlation matrices corresponding to the error bars, the extra white noise, and the red noise respectively, with a and b denoting the pulsar number, i and j denote the observation number, Δt is the TOA uncertainty (the error bar) as calculated in the pipeline, E_a is the scaling parameter of the error bars for the a'th pulsar (the EFAC factor), N_a is the amplitude of the white noise, R_a is the amplitude of the red timing noise, α_a is the spectral index of the red noise spectrum of pulsar a, and τ is the time difference between two observations.

4.4 Combining data sets

The previous section gives a complete description of the model we use to analyse the TOAs of a single pulsar, observed with one telescope. That model does not yet account for the use of different observatories. In this section we explain what we do to accomplish this.

As discussed in Section 2, the reduced data products are (sometimes subtlety) influenced by many different components of the reduction process. In order to account for slight offsets between TOAs, introduced by using slightly different reduction procedures on individual data sets, a calibration term needs to be introduced when merging TOAs from different observing systems. This extra calibration term takes the form of a 'jump', an arbitrary phase offset between data sets, which is fit for simultaneously with other timing model parameters. We use the term data set for any series of TOAs that can be analysed without a jump. In practice this is any series of TOAs, of the same pulsar, observed with the same hardware elements, and processed with the same algorithms, at the same observing frequency. Here we combine seven such data sets (those shown in Fig. 2).

Jumps have been used routinely when combining data of different observatories and/or data recorders (e.g. Janssen 2009). This allows us to find a single solution for the timing model of a pulsar timed by multiple observatories. However, the TOAs produced by pipelines at different observatories may have different statistical properties. In order to account for this, we allow the stochastic contributions in our model discussed in Section 4.3 to vary between data sets:

(1) one timing model per pulsar (taken directly from TEMPO2),
(2) jumps between different data sets,
(3) a scaling factor for the error bars (EFAC) for each data set,
(4) an extra white noise component (EQUAD) for each data set,
(5) power-law red noise for each data set.

A major advantage of this approach is that it allows one to detect statistical differences between observatories that may be introduced by different algorithms/components, and then use this feedback to iteratively improve our data sets.

The analysis of the TOAs consists of two steps. In the first step TEMPO2 is used to find the timing solution for a single pulsar. This includes possible jumps between data sets. Once the timing solution

is obtained, the results are passed on to the Bayesian algorithm. The Bayesian algorithm then analytically marginalizes all parameters of the timing model, including jumps, while using MCMC to explore the rest of the parameter space.

5 RESULTS

Now that we have developed the necessary framework to analyse the TOAs, we apply the algorithm to the observations. In the following subsections we explain in detail how we selected the five pulsars that we already mentioned in Section 3.2, and we present the GWB upper limit we are able to calculate using observations of those pulsars.

5.1 Selecting the most constraining data sets

For any pulsar, obtaining the timing solution and timing residuals is the first step after obtaining the TOAs. The timing residuals of the pulsars used in this work are shown in Fig. 2, and the parameters of the timing model are shown in the appendix. The timing model also includes several jumps as some of these pulsars have been observed with several European telescopes. The timing solutions we find are quite consistent with the values already published in the literature. Given that we are solving for 56 parameters, it is to be expected that one or two parameters deviate at the 2σ level. The only unexpected outlier we find is the proper motion in right ascension of J1713+0747, which deviates from Splaver et al. (2005) by over 5σ. Given that we are combining data of several telescopes, and that we do not take into account our red noise models in listing these timing solutions, we postpone exploring this difference to future work where the focus lies on investigating the statistics of the timing model parameters in the presence of red noise. Such an investigation is beyond the scope of this manuscript.

With the model of the systematic contributions in place, we first perform the analysis separately for each of the data sets and obtain the posterior probability distribution for their intrinsic noise parameters, specified in equation (7) of the previous section. Note that at this stage of the analysis the contribution from a GWB is not yet included. We determine a marginalized posterior for each pulsar as a function of the following parameter combinations:

(1) EFAC versus EQUAD,
(2) red noise amplitude versus red noise spectral index.

In both cases, the posterior is marginalized over all parameters but two, and the resulting two-dimensional distribution is displayed as contours at the 1σ, 2σ and 3σ level (the regions where respectively 68, 95 and 99.7 per cent of the volume of the posterior is enclosed).

As an example we consider the TOAs of pulsar J1713+0747, which consist of data taken with Effelsberg and Westerbork. Here we focus on the marginalized posterior distributions that represent information about the Effelsberg TOAs; these distributions and the residuals are shown in Figs 3 and 4. A traditional non-Bayesian analysis of the Effelsberg TOAs consists of a fit to the timing model with TEMPO2, which yields the best-fitting parameters, the corresponding uncertainties, and a reduced χ^2 statistic. The reduced χ^2 is defined as:

$$\chi^2 = \frac{1}{n-m} \sum_{i=1}^{n} \frac{\left(t_i^{\mathrm{obs}} - t_i^{\mathrm{fit}}\right)^2}{\epsilon^2 \sigma_i^2}, \tag{8}$$

where n is the number of observations, m is the number of free parameters in the least-squares fit, t_i^{obs} is the observed TOA, t_i^{fit} is
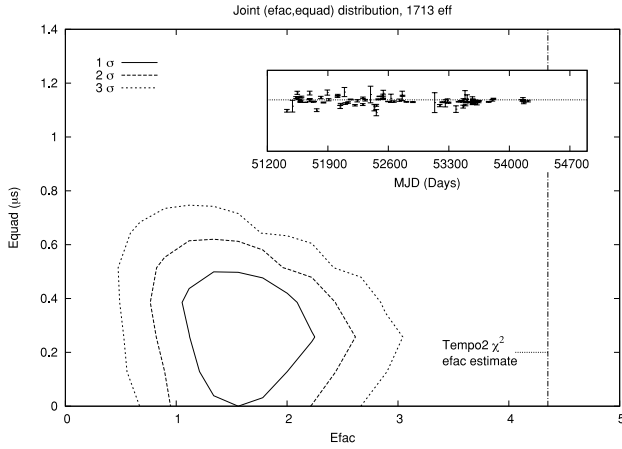
Figure 3. The marginalized posterior of J1713+0747 (Effelsberg), as a function of the EFAC and EQUAD parameters. The contours are at the 1σ, 2σ and 3σ level, indicating a respective volume inside that region of 68, 95 and 99.7 per cent.
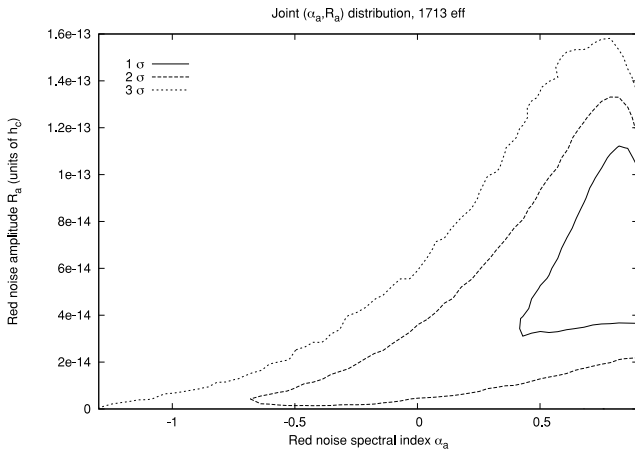

Figure 4. The marginalized posterior of J1713+0747 (Effelsberg), as a function of the power-law red noise parameters: the amplitude and the spectral index. The contours are at the 1σ, 2σ and 3σ level, indicating a respective volume inside that region of 68, 95 and 99.7 per cent.

best-fitting value of the TOA, σ_i is the TOA uncertainty of t_i^{obs}, and ϵ is the EFAC value. It is usual practice to set the EFAC such that the reduced $\chi^2 = 1$, which is accomplished by: $\epsilon = \sqrt{\chi^2(\epsilon = 1)}$. For the J1713+0747 Effelsberg TOAs, we have $\chi^2(\epsilon = 1) = 18.9$ and therefore $\epsilon = 4.35$.

As can be seen from Fig. 4, a non-zero red noise component is required to describe the TOAs. The EQUAD parameter is consistent with 0-amplitude according to Fig. 3, while the EFAC parameter is significantly lower than what a TEMPO2 $\sqrt{\chi^2}$ estimate would give. This tells us that no separate white-noise component is required to describe the TOAs: all the uncorrelated scatter can be assigned to the error bars on the TOAs. It is also of interest that in this case the EFAC parameter is much smaller, and indeed much closer to 1, than the more traditional estimator $\sqrt{\chi^2}$. The data is reasonably well modelled by just the presence of red noise.

It is also worth noting that, due to practicalities having to do with hardware changes at the observatories, the TOAs of J1713+0747 end at an earlier epoch than the other four pulsars. Although in the future the inclusion of this data will obviously benefit the sensitivity

to the GWB, we note that the GWB limit is not negatively effected by this lack of overlap of the TOAs between pulsars.

The analysis of the TOAs of the other pulsars yields similar, but slightly different results. As can be seen in the appendix, some pulsars do have non-negligible white noise, and some do appear to have EFAC values significantly different from 1. As of yet we do not have a complete explanation for the exact form of the marginalized posteriors.

We present the marginalized posterior as a function of the red noise parameters in an intuitive way: as pointed out in Section 3.2 we use the same units for the red noise amplitude and red noise spectral index as we use for the GWB parameters. For the analysis of TOAs of just one pulsar, the red noise can now be thought of as if it was generated solely by a GWB with a certain amplitude and spectral index. In this case, the marginalized posterior for the red noise parameters shows us what upper limit we are able to place on the GWB amplitude as a function of spectral index.

We choose a 3σ threshold of $R_a \leq 10^{-13}$ at a spectral index of $\alpha_a = -2/3$. Based on the marginalized posteriors of all the EPTA pulsars, we can decide whether a particular data set can put a constraint on the GWB lower than this or not. Using this threshold we include five pulsars in our final analysis. These five significantly outperform the other pulsars in terms of how well they can limit the GWB amplitude, and we do not expect to gain any significant sensitivity by including more pulsars in our current archival data sets. The residuals of the pulsars we use in our combined analysis are shown in Fig. 2. More data sets will be added after some extensive and detailed recalibration procedure of existing data sets.

5.2 GWB upper limit

Now that we have selected our pulsars that can significantly contribute to a GWB limit, we are in the position to infer the amplitude and spectral index of the GWB. Our model of the combined data of the five pulsars we selected in Section 5.1 consists of all sources we included in the analysis for the single pulsars, and an extra source that corresponds to the GWB. As discussed in Section 4.3, the GWB source is a power-law correlated between pulsars as described by equation (4).

As before, we use MCMC to sample the posterior distribution while analytically marginalizing over the timing model; now the analytic marginalization happens simultaneously for the timing models of the five pulsars. In Fig. 5 we present the posterior, marginalized over all parameters except the GWB amplitude and spectral index. In the same figure we also show the PPTA published values of the GWB limit (Jenet et al. 2006). For the expected spectral index for a GWB generated by a large number of supermassive black hole binaries, $\alpha = -2/3$, we find a 95 per cent confidence GWB upper limit of $h_c(1\mathrm{yr}) \leq 6 \times 10^{-15}$. This is smaller by a factor of 1.8 than the previously published PPTA limit.

As a cross-check with other codes, and to verify that we are definitely sensitive to the level of the limit we have calculated here, we perform an additional test. We use the TEMPO2 plug-in GWbkgrd (Hobbs et al. 2009) to generate simulated timing residuals as produced by a GWB with an amplitude of $h_c(1\mathrm{yr})$. We then create a new set of TOAs, consisting of the values of the simulated timing residuals added to the values of the observed TOAs of the five pulsars that we have analysed in this section. We then redo the whole analysis. Current PTAs aim to reach sensitivities in the order of $h_c(1\mathrm{yr}) = 10^{-15}$ in the future (Jenet et al. 2005), which is over five times more sensitive than the limit we achieve here. In the case that the GWB just happens to be at the 2σ level of our current
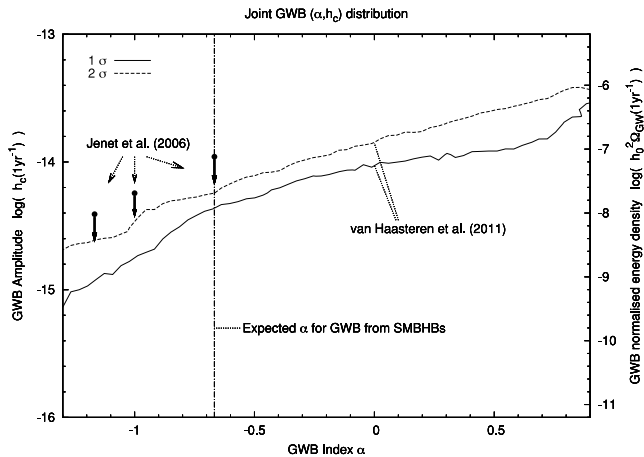
Figure 5. The marginalized posterior distribution as a function of the GWB amplitude, and spectral index. The contours marked by 'van Haasteren et al. (2011)' are the results of this work at the 1σ and 2σ level, indicating a respective volume inside that region of 68 and 95 per cent. The vertical dot–dashed line at $\alpha = -2/3$ shows where we expect a GWB generated by supermassive black hole binaries. The most recent published limits are shown as the three upper limit arrows pointing down, marked by 'Jenet et al. (2006)'.
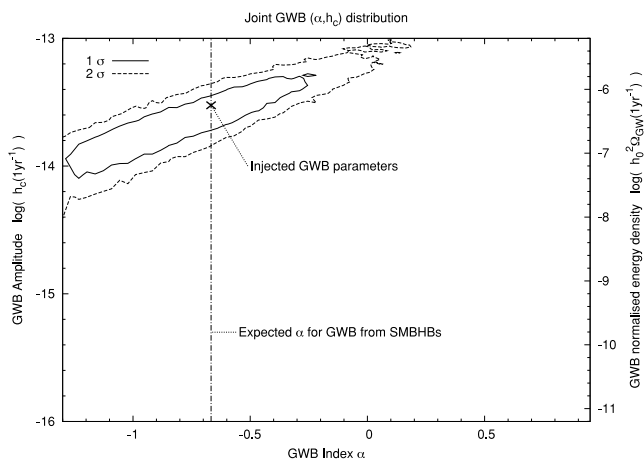
Figure 6. Same marginalized posterior distribution as in 5, but here we have injected the residuals of a simulated GWB with amplitude $h_c(1\text{yr}) = 30 \times 10^{-15}$ in the data.

limit, we demonstrate what such a five-fold increase in sensitivity could do for our ability to measure the GWB parameters by adding a signal of $h_c(1\,\text{yr}) = 30 \times 10^{-15}$ to our current TOAs. The result is shown in Fig. 6. We find that the results are consistent with the input parameters of the simulated GWB, and that we can reliably detect a GWB in this case.[3] The values of the GWB parameters we have used to simulate the GWB lie within the 1σ credible region of Fig. 6.

6 IMPLICATIONS

The analysis performed in this work puts an upper limit on a GWB with a power-law characteristic strain spectrum $h_c = A(f/\text{yr}^{-1})^{\alpha}$.

---

[3] We note that, although such a detection is consistent with a GWB, we would need more pulsars to exclude the possibility that some other effect is causing the correlated signal we detect here.

In the literature, upper limits are typically quoted for various values of α, where the considered α depends on the physics responsible for generation of the GWB. A useful feature of our approach is that we are able to measure α for a strong enough GWB (see vHLML for a discussion). The extra degree of freedom in our model, α, necessarily changes the interpretation of the posterior to some extent. We interpret the 2σ contour in our plot of the marginalized posterior as the upper limit on the GWB as a function of α. Fixing α and re-evaluating the 2σ limit based on the posterior for A only does not significantly alter our results.

In this section, we briefly discuss the implications of the new upper limits in the context of two different mechanisms for generation of the GWB: binaries of supermassive black holes and cosmic strings.

6.1 Supermassive black hole binaries

Several authors discuss the characteristic strain spectrum generated by an ensemble of supermassive black holes (SMBHBs) distributed throughout the Universe (Begelman et al. 1980; Phinney 2001; Jaffe & Backer 2003; Wyithe & Loeb 2003). They show that the characteristic strain spectrum generated by such black hole binaries can well be approximated by a power law:

$$h_c = h_{1\text{yr}} \left(\frac{f}{\text{yr}^{-1}} \right)^{-2/3}, \qquad (9)$$

where $h_{1\text{yr}}$ is a model-dependent constant. Though the form of the characteristic strain, the power law, is quite general among the different SMBHB assembly models the authors use in their work, the parameterizations and assumptions about other physical quantities differ between all investigators. The predicted $h_{1\text{yr}}$ therefore differs depending on what SMBHB assembly scenarios were assumed.

Recently, Sesana et al. (2008) have extensively investigated a wide variety of assembly scenarios, including those considered in Jenet et al. (2006). For our purposes in this work, their most important result is an estimate of $h_{1\text{yr}}$ for all models. In calculating this value, they take into account the uncertainties of the key model parameters for different scenarios, and come up with $h_{1\text{yr}} \approx 2 \times 10^{-16}$ to 4×10^{-15}. We are less than a factor of 2 away from this range, so we foresee that we can start to rule out some models in the near future.

Two more results of Sesana et al. (2008) are interesting with respect to the limit presented in this work. The first is that the frequency dependence of the GWB is expected to be steeper than a power law $\propto f^{-2/3}$ for frequencies $f \gtrsim 10^{-8}$ Hz. The steepness depends on the chosen model. We have incorporated a varying spectral index α in our current analysis, and since we are not yet able to detect the GWB, we postpone a more thorough investigation of the exact dependence of h_c on f to later work with even better data sets. The second interesting result is that in the frequency range of 10^{-8} Hz $\leq f \leq 10^{-7}$ Hz, the GWB might be dominated by single sources. In that case, a search for just a certain characteristic strain spectrum is not appropriate, and we note that further investigation is required in this regard.

6.2 Cosmic strings

Several authors have suggested that oscillating cosmic string loops will produce GWs (Vilenkin 1981; Damour & Vilenkin 2005; Ölmez et al. 2010). Damour & Vilenkin (2005) have used a semi-analytical approach to derive the characteristic strain h_c of the GWB

generated by cosmic strings:

$$h_c(f) = 1.6 \times 10^{-14} c^{1/2} p^{-1/2} \epsilon_{\text{eff}}^{-1/6}$$
$$\times (h/0.65)^{7/6} \left(\frac{G\mu}{10^{-6}} \right)^{1/3} \left(\frac{f}{\text{yr}^{-1}} \right)^{-7/6}, \quad (10)$$

where μ is the string tension, G is Newton's constant, c is the average number of cusps per loop oscillation, p is the reconnection probability, ϵ_{eff} is the loop length scale factor and h is the Hubble constant in units of $100 \, \text{km s}^{-1} \, \text{Mpc}^{-1}$. Usually, the dimensionless combination $G\mu$ is used to characterize the string tension. Theoretical predictions of string tensions are $10^{-11} \leq G\mu \leq 10^{-6}$ (Damour & Vilenkin 2005).

From the above expression for the characteristic strain generated by cosmic strings, we see that this is again a power law, but now with $\alpha = -7/6$. Using a standard model assumption that $c = 1$, the facts that p and ϵ_{eff} are less than one, and that h is expected to be greater than 0.65, we can safely use our derived upper limit on h_c for $\alpha = -7/6$ to limit the string tension: $G\mu \leq 4.0 \times 10^{-9}$. This already places interesting constraints on the theoretical models, and in a few years the EPTA will be able to place much tighter restrictions in the case of a non-detection of a GWB: with only a factor of five decrease of the upper limit, we would be able to completely exclude the $10^{-11} \leq G\mu \leq 10^{-6}$ range mentioned in Damour & Vilenkin (2005).

7 CONCLUSION AND DISCUSSION

In this paper we have developed the methodology on how to handle combined PTA data sets of several telescopes and how to robustly calculate a corresponding upper limit on the GWB. Our Bayesian approach has handled in a straightforward way different data sets of varying duration, regularity, and quality. The current upper limit on the GWB, calculated with EPTA data, is $h_c \leq 6 \times 10^{-15}$ in the case of $\alpha = -2/3$, as predicted for a GWB by an ensemble of supermassive BH binaries. More generally, the analysis has resulted in a marginalised posterior as a function of the parameters of the GWB: the GWB amplitude and the spectral index.

Due to hardware and software upgrades at the EPTA observatories, and due to the ever increasing time baseline of the data, we expect the sensitivity to increase greatly over the next few years. Especially the combination of the EPTA data sets with the data of the other PTA projects seems promising.

The raw telescope data must first undergo careful reduction and modelling before it can be analysed by the Bayesian algorithm. We have provided some discussion of these processes and have motivated our choice of model for the TOAs. As part of our analysis, we have studied the probability distribution of the pulsar noise parameters, and highlighted the crucial importance of precise characterization of the red component of pulsar timing noise.

ACKNOWLEDGMENTS

REFERENCES

Begelman M. C., Blandford R. D., Rees M. J., 1980, Nat, 287, 307
Cordes J. M., Shannon R. M., 2010, preprint (arXiv:1010.3785)
Damour T., Vilenkin A., 2005, Phys. Rev. D, 71, 063510
Detweiler S., 1979, ApJ, 234, 1100
Estabrook F., Wahlquist H., 1975, Gen. Relativ. Gravitation, 6, 439
Foster R., Backer D., 1990, ApJ, 361, 300
Grishchuk L. P., 2005, Uspekhi Fizicheskikh Nauk, 48, 1235
Hellings R., Downs G., 1983, ApJ, 265, L39
Hobbs G. B., Edwards R. T., 2006, TEMPO2 user manual, Version 2.0
Hobbs G. B., Edwards R., Manchester R., 2006, Chinese J. Astron. Astrophys. Suppl., 6, 020000
Hobbs G. B. et al., 2009, Publ. Astron. Soc. Australia, 26, 103
Hobbs G. B. et al., 2010, Class. Quantum Grav., 27, 084013
Jaffe A., Backer D., 2003, ApJ, 583, 616
Janssen G. H., 2009, PhD thesis, Univ. Amsterdam
Jenet F., Hobbs G., Lee K., Manchester R., 2005, ApJ, 625, L123
Jenet F. et al., 2006, ApJ, 653, 1571
Jenet F. et al., 2009, preprint (arXiv:0909.1058)
Kaspi V. M., Taylor J. H., Ryba M. F., 1994, ApJ, 428, 713
Lazaridis K. et al., 2009, MNRAS, 400, 805
Lommen A. N., 2002, in Becker W., Lesch H., Trumper J., eds, WE-Heraeus Seminar on Neutron Stars, Pulsars and Supernova Remnants, Garching, MPE, p. 114
McHugh M. P., Zalamansky G., Vernotte F., Lantz E., 1996, Phys. Rev. D, 54, 5993
Maggiore M., 2000, Phys. Rep., 331, 283
Ölmez S., Mandic V., Siemens X., 2010, Phys. Rev. D, 81, 104028
Phinney E. S., 2001, preprint (astro-ph/0108026)
Sazhin M. V., 1978, Soviet Astron., 22, 36
Sesana A., Vecchio A., Colacino C. N., 2008, MNRAS, 390, 192
Splaver E. M., Nice D. J., Stairs I. H., Lommen A. N., Backer D. D, 2005, ApJ, 620, 405
Stinebring D. R., Ryba M. F., Taylor J. H., Romani R. W., 1990, Phys. Rev. D, 65, 285
Taylor J. H., 1992, Philos. Trans. Royal Soc. London, 341, 117
Tofani G. et al., 2008, in SPIE Conf. Ser. Vol. 7012, Status of the Sardinia Radio Telescope Project. SPIE, Bellingham
van Haasteren R., Levin Y., McDonald P., Lu T., 2009, MNRAS, 395, 1005
Verbiest J. P. W. et al., 2010, Class. Quantum Grav., 27, 084015
Vilenkin A., 1981, Phys. Lett. B, 107, 47
Wyithe J., Loeb A., 2003, ApJ, 595, 614

APPENDIX A:

Here we show the timing solutions (see Table A1) of all data sets used in this work, combined with the posterior distributions (Figs A1 & A2) for the timing noise.
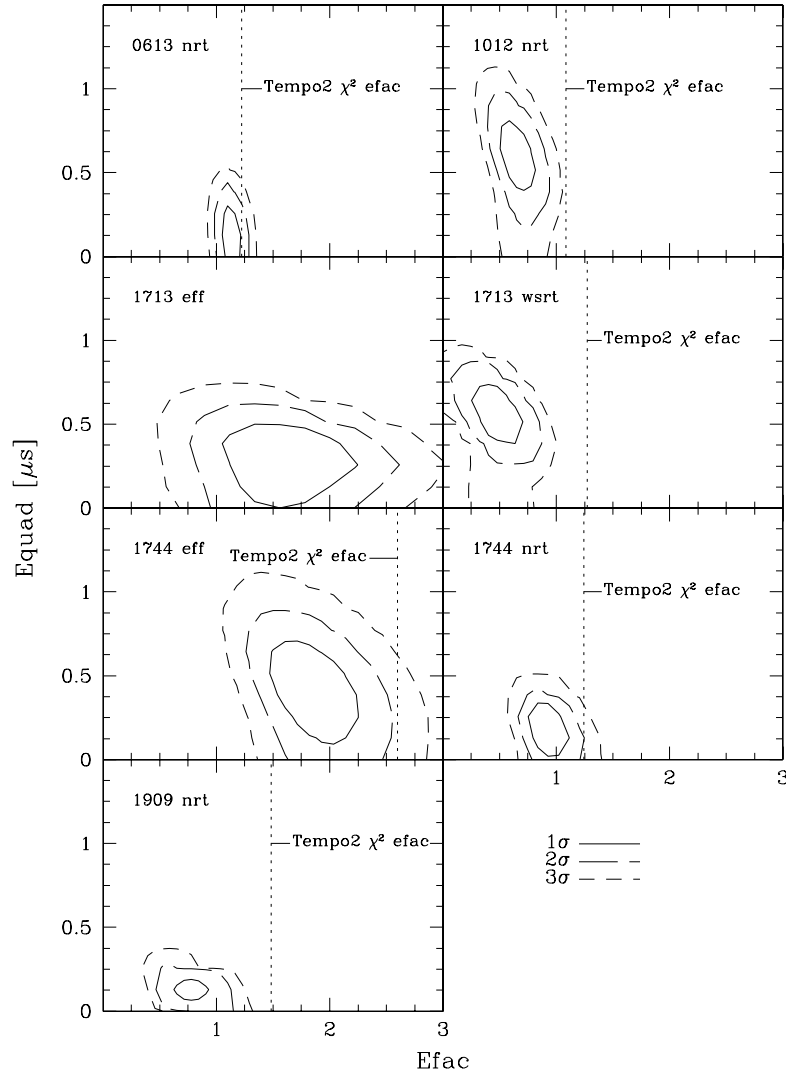
Figure A1. The marginalized posteriors of all data sets, as a function of the EFAC and EQUAD parameters. The contours are at the 1σ, 2σ and 3σ level, indicating a respective volume inside that region of 68, 95 and 99.7 per cent. For the J1713-0747 posterior, the TEMPO2 χ^2 estimate is not shown because it has the off-scale value of 4.4.
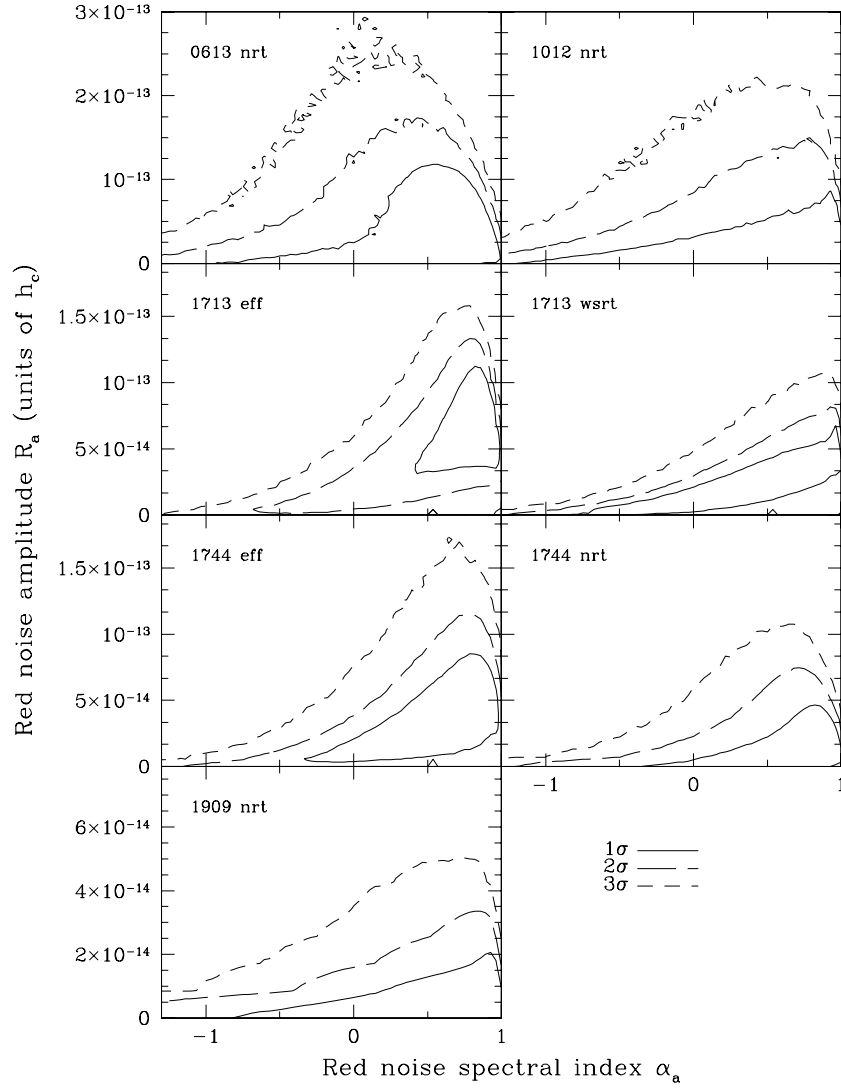
Figure A2. The marginalized posterior of all data sets, as a function of the power-law red noise parameters: the amplitude and the spectral index. The contours are at the 1σ, 2σ and 3σ level, indicating a respective volume inside that region of 68, 95 and 99.7 per cent. The more negative the value of α, the steeper the power-law spectrum, with the spectrum approaching a white spectrum at the right of the plot. We also note that the amplitude of the red noise cannot be trivially scaled linearly to an rms value of the timing residuals.

Table A1. The timing solutions for the pulsars used in this paper before applying the Bayesian algorithm. These solutions are determined using TEMPO2, which uses the International Celestial Reference System and Barycentric Coordinate Time. As a result this timing model must be modified before being used with an observing system that inputs TEMPO format parameters. See Hobbs et al. (2006) for more information. Note that the figures in parentheses are the nominal 1σ TEMPO2 uncertainties, with EFACs included, and therefore do not include the red noise model. In the GWB limit calculation these respective parameters are marginalized over. Also, the dispersion measure quoted here results from combining these observations with EPTA data of other frequencies. These DM values are used in the de-dispersion, but we did not include all observations in our GWB analysis. We therefore have not fit for the DM here, and an error estimate cannot be given.

Pulsar name	J0613−0200	J1012+5307	J1713+0747	J1744−1134	J1909−3744
Fit and data set					
Telescopes used	NRT	NRT	EFF and WSRT	EFF and NRT	NRT
MJD range	53367–55012	53443–55030	51426–54637	51239–55001	53366–55127
Number of TOAs	280	107	195	159	113
Rms timing residual (ns)	912	769	396	444	134
Reduced χ^2 value	1.00	1.00	1.13	1.05	1.00
Epoch	54 189	54 236	53 031	53 120	54 247
Measured Quantities					
RA, α (J2000)	06:13:43.97385(4)	10:12:33.43241(10)	17:13:49.530782(3)	17:44:29.391592(7)	19:09:47.437982(5)
Dec., δ (J2000)	−02:00:47.0720(12)	+53:07:02.665(2)	+07:47:37.52343(8)	−11:34:54.5762(6)	−37:44:14.3176(2)
Pulse freq., ν (s^{-1})	326.600 562 095 168(13)	190.267 834 482 48(14)	218.811 840 486 637(30)	245.426 119 777 227(4)	339.315 687 323 55(1)
Derivative of pulse freq., $\dot{\nu}$ (s^{-2})	−1.022 81(3) × 10^{-15}	−6.1998(4) × 10^{-16}	−4.0836(2) × 10^{-16}	−5.3817(4) × 10^{-16}	−1.614 853(8) × 10^{-15}
PM in RA, μ_α (mas yr^{-1})	1.90(4)	3.17(7)	5.017(12)	18.817(10)	−9.490(11)
PM in Dec., μ_δ (mas yr^{-1})	−10.31(9)	−24.96(9)	−3.96(3)	−9.30(6)	−35.89(4)
Parallax, π (mas)	–	–	0.915(7)	2.602(10)	1.01(7)
Dispersion measure, DM (cm^{-3}pc)	38.77700	9.0176	15.9907	3.13632	10.37877
Binary model	DD	ELL1	DD	–	ELL1
Orbital period, P_b (d)	1.198 512 575 34(5)	0.604 622 723 22(4)	67.825 330 9255(20)	–	1.533 499 474 90(6)
Derivative of orbital period, $\dot{P}_b$	–	–	–	–	3.5(5) × 10^{-13}
Epoch of periastron, T_0 (MJD)	54 189.019(6)	–	53 014.9592(7)	–	–
Projected sm. axis of orbit, x (lt-s)	1.091 444 17(8)	0.581 817 42(13)	32.342 420 15(7)	–	1.897 991 08(11)
Longitude of periastron, ω_0 (°)	47.1(1.6)	–	176.2109(12)	–	–
Orbital eccentricity, e	5.47(15) × 10^{-6}	–	7.493 12(13) × 10^{-5}	–	–
Time of ascending node (MJD)	–	54 236.207 8302(3)	–	–	54 247.169 903 748(15)
EPS1 (ϵ_1), $e\sin\omega$	–	1.18(5) × 10^{-5}	–	–	6.4(5.5) × 10^{-8}
EPS2 (ϵ_2), $e\cos\omega$	–	2.20(5) × 10^{-5}	–	–	−3(3) × 10^{-8}
Sine of inclination angle, $\sin i$	–	–	–	–	0.9980(3)
Companion mass, M_c (M$_\odot$)	–	–	–	–	0.208(7)
Assumptions					
Clock correction procedure			TT(TAI)		
Solar system ephemeris model			DE405		

This paper has been typeset from a TEX/LATEX file prepared by the author.